How to Cite:
Indira, S., & Kannaian, T. (2022). Analysis of DC motor driven laparoscopic device for oncology. *International Journal of Health Sciences*, *6*(S2), 2289–2301.
https://doi.org/10.53730/ijhs.v6nS2.5332

Analysis of DC motor driven laparoscopic device for oncology

Indira S
Assistant Professor, Department of Electronics, Sri Ramakrishna College of Arts and Science, Coimbatore, Tamilnadu, India
Email: indiras1987@gmail.com

Kannaian T
Secretary, PSG College of Arts and Science, Coimbatore, Tamilnadu, India
Email: kannaian@gmail.com

***Abstract*---**In every hospitals Patient handling equipment Laparoscopic, high-quality pumps, centrifuges, infusion pumps, insulin pumps, hemodialysis machines, compressors, respirators, scanners, dental drills, precision surgical hand pieces, surgical robot grippers, prosthesis and implantable devices (ventricular assist devices, pacemakers, defibrillators, nerve stimulators, and so on) are needed small electric motors. Electric motors are also very essential in healthcare equipment, such as exercisers, wheelchairs, massage machines, treatment machines, and so on. This research work focuses on Laparoscopic device, in this device very compact DC motor is used. In this research work the electrical and mechanical characteristics of Compact DC motors are analyzed. The simulation work was done in MATLAB simulation and results are discussed.

***Keywords*---**DC motor, laparoscopic, mechanical, electrical characteristics.

Introduction

The medical field has been transformed by the advent of robot-assisted surgery into the operating room. These systems not only provide the benefits of traditional Minimally Invasive Surgery (MIS), such as reduced patient trauma and recovery time, lower morbidity, and lower health-care costs, but they also eliminate surgeon tremor, reduce the effects of surgeon fatigue, and allow remote surgical procedures to be performed. However, when compared to traditional MIS, existing systems have flaws such as high cost, inability to use qualitative data, and lack of hepatic input to the surgeon. These solutions have included the addition of

International Journal of Health Sciences ISSN 2550-6978 E-ISSN 2550-696X © 2022.
***Corresponding author**: Indira, S.; Email: indiras1987@gmail.com*
Manuscript submitted: 27 Jan 2022, Manuscript revised: 18 Feb 2022, Accepted for publication: 09 March 2022

sensors, such as strain gauges, to indirectly record the forces at the tool tip. Researchers have also used sensors in the design of new laparoscopic instruments or systems to incorporate force feedback. These designs have sensors that are situated distance from the tool tip and measure the forces at the tip indirectly or just measure one resolved force on the tool. A direct sensing method for tissue characterization using pressure measurements normal to the surface of the jaws has also been added. These approaches, however, are costly, non-sterilisable, and non-modular, making them challenging to include into laparoscopic instruments. While increasing the feedback gain several times might eliminate friction in the mechanism, it would also cause in-exact forces to be felt by the surgeon, making the overall system less transparent.

Speed-Torque Characteristics

A DC motor is defined by two torque parameters: peak torque and rated torque. The motor can be loaded up to rated torque during continuous operations. This is a short-term requirement, especially when the motor begins from a standstill or accelerates. Extra torque is required at this time to overcome the inertia of the load and the rotor itself. As long as the motor follows the speed torque curve, it can provide increased torque up to maximum peak torque. The continuous torque zone is maintained while the speed climbs to the maximum value of torque of the motor, up to the rated speed. After exceeding the rated speed, the torque of the motor drops. The stall torque is the torque at which the shaft is not rotating but the torque is at its highest. The no-load speed is the motor's maximum output speed. The voltage effectively controls the speed, which may be changed by changing the supply voltage. PWM is commonly used to manage the voltage, which results in a variety of torque/speed characteristics at the intersections of continuous and intermittent operation.

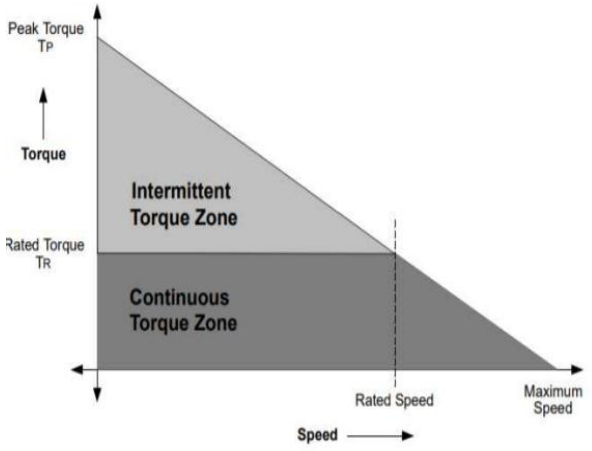

Figure 1 Speed-Torque characteristics

The speed torque characteristics of a DC motor are shown in the diagram below. Heat transfer and temperature rise are commonly used to calculate the continuous limit. Temperature rise or the maximum ratings of semiconductor devices in the controller can determine the intermittent limit.

Basic Block Diagram

The block diagram of DC motor driven Laproscopic device is shown figure 2. H-bridge circuit will help to control the DC motor function of direction. Design engineers will find that the combination of compact size, light weight, and low power, as well as integration possibilities for pump and motor units in medical devices, provides a perfect solution. They may now develop a more portable device that delivers all of the performance their clients need in a smaller compact.

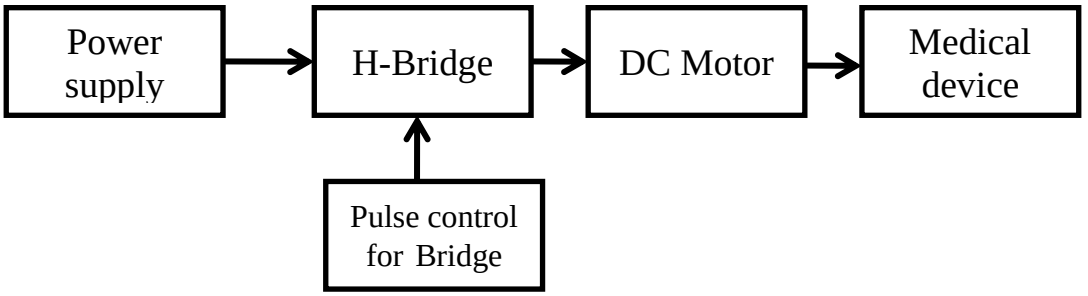

Figure 2 Functional block diagram DC Motor Driven Laparoscopic device

The power supply was DC and the H-Bridge is used to control the motor direction and also the speed of the rotor. Pulse Control Bridge will control the speed and all the functions.

Brushed Direct Current Motor Modelling

The DC motor is a typical actuator in the Medical environment, and understanding how to choose the MOSFETs that control it and their ratings, as well as obtaining the desired behavior from the motor, is important.

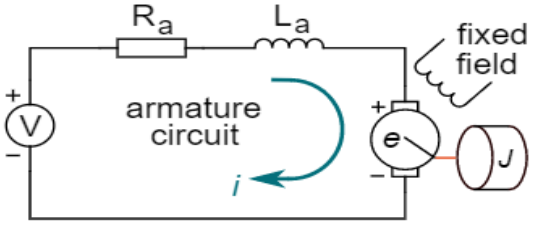

Figure 3 Motor armature equivalent circuits

A DC motor is powered by a 5 V DC voltage source. The armature circuit of a DC motor can be considered while looking at its internal construction shown in figure 3.2. Its electric resistance (Ra), inductance (La), and back EMF are all included in this (e). Also displayed are the rotor mechanical constants: motor torque (T), rotor angle (θ), and rotor inertia (J). Eq. 1 is obtained by considering these factors and use circuit analysis techniques such as Kirchhoff's voltage law.

$$V = i \times R_a + L_a \frac{\mathrm{di}}{dt} + \mathrm{e} \qquad (1)$$

V is the DC motor's input voltage, as well as the one supplied by the H-bridge, which is made up of four MOSFETs arranged in two half-bridges to provide bi-directional control.

The torque produced by the DC motor will be proportional to the armature current and the motor torque constant KT if the magnetic field is assumed to be constant. This is illustrated in Eq. 2 below:

$$T = i \times K_T \tag{2}$$

As demonstrated in Eq. 3.3 below, the back EMF is proportional to the rotor velocity d θ/dt and the back EMF constant K:

$$e = K_e \times \frac{\mathrm{d}\theta}{\mathrm{d}t} = k \times \omega \tag{3}$$

Because the torque and back EMF constants are assumed to be equal, the following equality can be used: KT = Ke = K. Knowing the motor constants may be used to approximate the motor output torque and speed using the equations above.

H-Bridge Theory

The H-bridge, also known as the full-bridge, is a four-switch electrical system that can provide bidirectional current and reversible voltage across its load. When running a motor, this feature comes in handy because it allows you to change the direction of rotation and, if the application allows it, even utilize it as a generator. This circuit is found in a variety of systems, including DC/AC inverters, DC/DC regulators, and class-D amplifiers. The H-bridge is made up of two half-bridges that are employed at the same time. The half-bridge can handle bi-directional current but not reversible voltage, hence it's mostly utilized in single-direction motor drive applications like oil pump motors and small fans.

Modes of switching

Pulse width modulation is the simplest and most popular approach to drive a DC motor with an H-bridge (PWM). The MOSFETs are switched at a constant frequency with a variable duty cycle control signal. This permits the average voltage across the motor to change, allowing the rotor angular velocity to be controlled. To achieve the desired voltage polarity, the MOSFETs in an H-bridge can be switched in several sequences. Bipolar and unipolar modes are the most common.

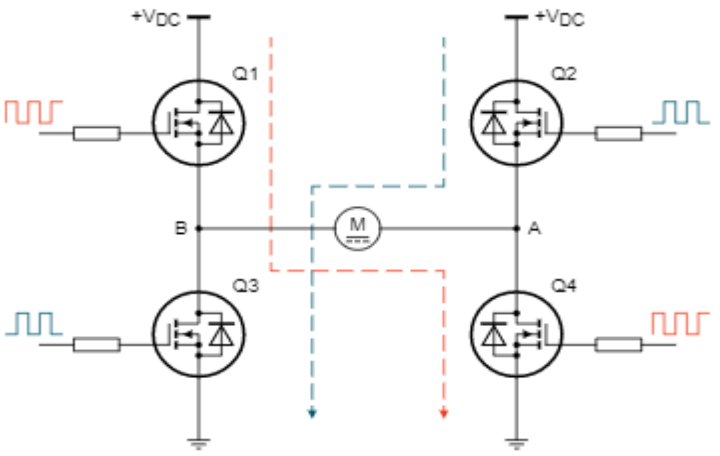

Figure 4 Bipolar drive H-bridge switching

Two MOSFETs can be turned on at the same time with the bipolar drive. Both Q2 and Q3 are turned on in the case of positive current (from node A to node B). Q1 and Q4 are switched on for negative current, whereas Q1 and Q4 are turned off for positive current. The current direction is selected by turning on one or both of the FETs while providing a voltage across the motor those changes between VDC and -VDC, with an average value that depends on the duty cycle (δ). To avoid cross-conduction (or shoot through), which shortens the supply, a time delay, known as dead-time, must be provided between the turning OFF of one pair and the turning ON of the other pair. Instead, the unipolar drive scheme allows the current to be managed by keeping one right-side MOSFET (Q2 or Q4) ON while only switching one left-side MOSFET (Q3 or Q1). It allows for the reduction of dead time, which minimizes the complexity of the driving circuit in its most basic form. When the switching MOSFET is turned off, some current will be forced to pass through one of the MOSFETs body diode for the same reason as in the bipolar drive.

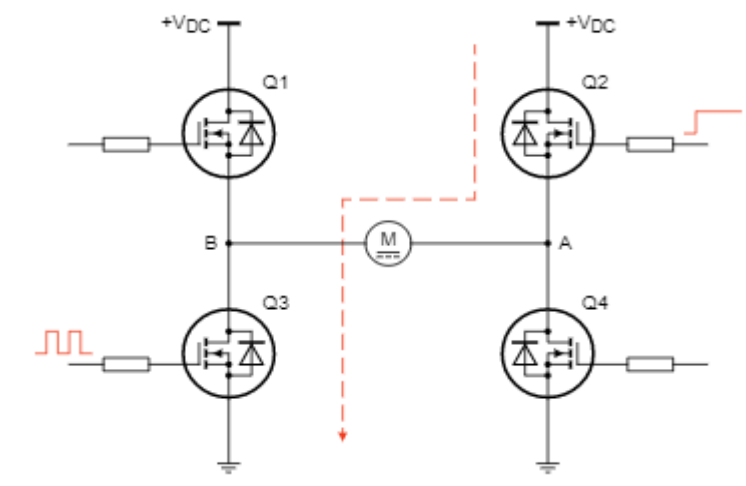

Figure 5 Unipolar drive H-bridge switching

Due to the magnetic field build-up in the motor, some current will continue to flow during the delay phase, even though all devices are turned off, by recirculation through the MOSFETs body diodes. If Q3 is switched on and Q2 is turned on, electricity will flow through Q1's body diode when the former is turned off. Q1 can be turned on while Q3 is turned off to reduce the loss produced by the diode voltage drop. A proper dead-time constraint must be observed in this scenario. The voltage across the motor will have an amplitude of just VDC, which is one of the key differences with the bipolar drive scheme. As a result, the peak of the ripple current through the motor is half that of the bipolar instance, resulting in fewer motor losses.

Motor Characterisation and Constants

To simulate the behavior of the H-bridge controller, the motor characteristics had to be extracted so that the rotor speed in the simulation matched those of the real application for a given PWM duty cycle. The rotor dimensions were measured, and the moment of inertia was calculated by fitting it to a cylinder using Eq. 4, where m = rotor mass and r = rotor radius.

$$\text{Moment of inertia } J = \frac{1}{2}\text{mr}^2 \quad (4)$$

The rotor was found to weigh 220 g and have a radius of roughly 17 mm, resulting in a moment of inertia of around 3.15x10-5 kgm^2. Furthermore, the plastic disc was discovered to have a moment of inertia of about 3.5x10-6 kgm^2. The overall inertia was determined to be 3.5x10-5 kgm^2 when the two were added together. The winding resistance was measured with a DMM to be around 1.5. This was also discovered by a motor stall test and the DC motor's step reaction, as shown in Fig 6.

$$\text{Winding resistance: R} = \frac{\text{V}_{\text{Steady state}}}{\text{I}_{\text{Steady state}}} = \frac{3.68\ \text{V}}{2.39\ A} = 1.54\ ohm \quad (5)$$

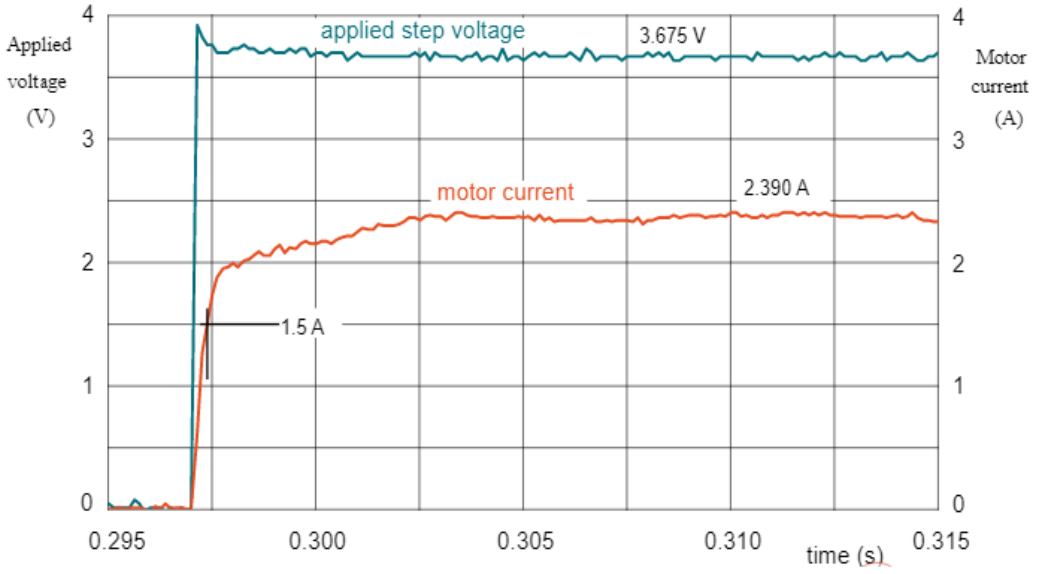

Figure 6 DC motor step response

Eq 6 is used to find the motor's electrical time constant. The current in Fig. 9 reaches approximately 1.5 A at 63.2 percent of its steady state value (Eq 7, Eq 8) This occurs at a rate of 0.39 milliseconds. The winding inductance was found to be roughly 600 H using and the value obtained for the motor winding resistance.

$$\text{Motor time constant: } \tau = \frac{\mathrm{L}}{\mathrm{R}} \tag{6}$$

$$i(t) = I_{ss}(1 - e^{\frac{t}{\tau}}) \tag{7}$$

$$t = \tau = i\,(\tau) = I_{ss}(1 - e^{-1}) = 0.632\, I_{ss} \tag{8}$$

The rotational speeds of the motor, as well as the currents and voltages, were discovered through a series of experiments. The motor's KV and Ke values were deduced from these, and the KT value was found to be around 0.045 Nm/A. The following are considered motor constants for DC motors in eqn 3.9

$$\text{Motor constants: } Kv = \frac{\omega_{\mathrm{no-load}}}{\mathrm{V}} \text{ also: } \mathrm{Kt} = \frac{1}{\mathrm{Kv}} \tag{9}$$

The real system achieved a rotational speed of around 6 RPS or 360 RPM, or around 37.7 rad/s. The voltage on the board was 20 V, the PWM frequency was 15.6 kHz, and the duty cycle was 12.5 percent.

Results and Discussion

In medical application the speed of motor and also the reversal of motor is very essential for surgical need. The performance of DC motor was simulated in MATLAB environment. The outputs are taken and made discussion. Figure 7 shows that the simulink model for analyzing the DC motor performance. The DC motor output speed is taken as feedback signal and given to the controller block, in controller block the reference speed is compared with the actual measured

speed of the DC motor and creates the error signal like positive error or negative error. based on the error signal PWM pulses are generated and given to the DC-DC controller, the controller activates the H bridge based on the input and change the direction of operation.

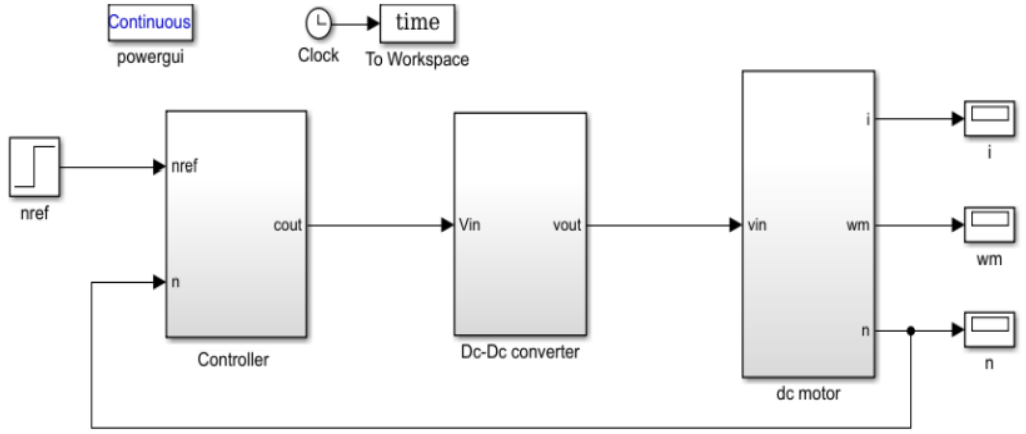

Figure 7 Simulink model of DC motor

The output wave form of reference speed vs measured speed shown in figure 8. In that waveform from time period 0 sec to 0.2 sec the speed is trying to maintain 50 rpm but the time 0.025 sec motor will take time to reach desired speed. Likewise the time period 0.2 sec the reference speed is 120 rpm, again at the time period of 0.4 sec motor speed decreased to 80 pm and 0.6 sec the motor reference speed will be 150 rpm. From that wave form each and every time the actual speed will take some delay to meet reference speed.

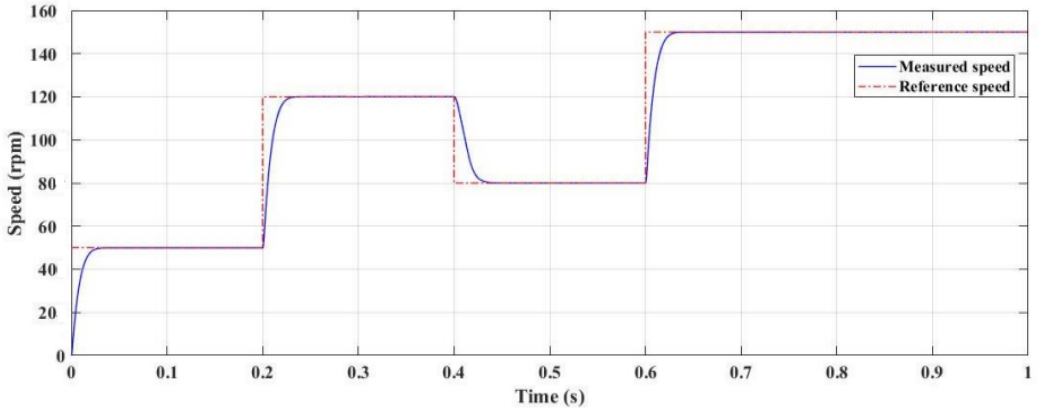

Figure 8 Speed responses to the step change reference speed

The Figure 9 shows that the Speed response to the step change load torque. Whenever changing the speed of the motor in reference feed, the torque of the DC motor also changed. The impulse change of the torque will leads to make small

disturbance in medical application. Because even 0.5 n-m torque also make major change in output performance.

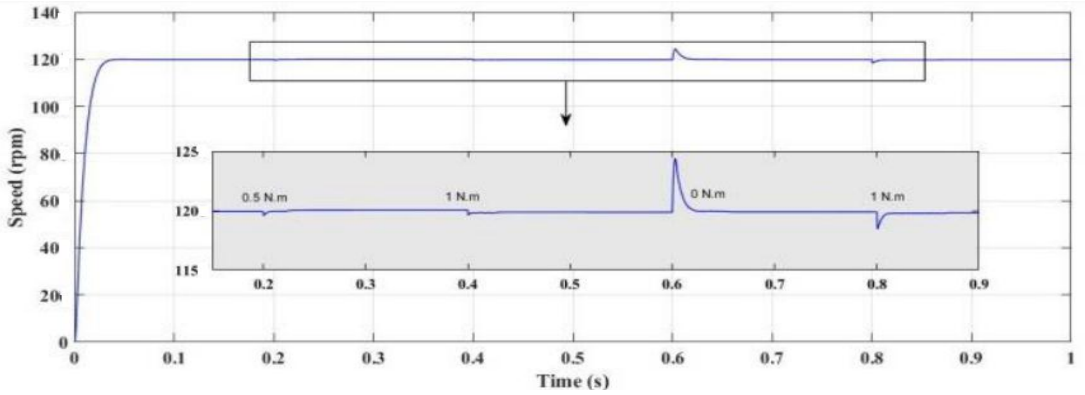

Figure 9 Speed response to the step change load torque

Figure 10 shows that the current responses to the step change load torque, if we need to change the DC motor speed we need to make armature control method or field control method. Both the methods the current of motor also makes major disturbances.

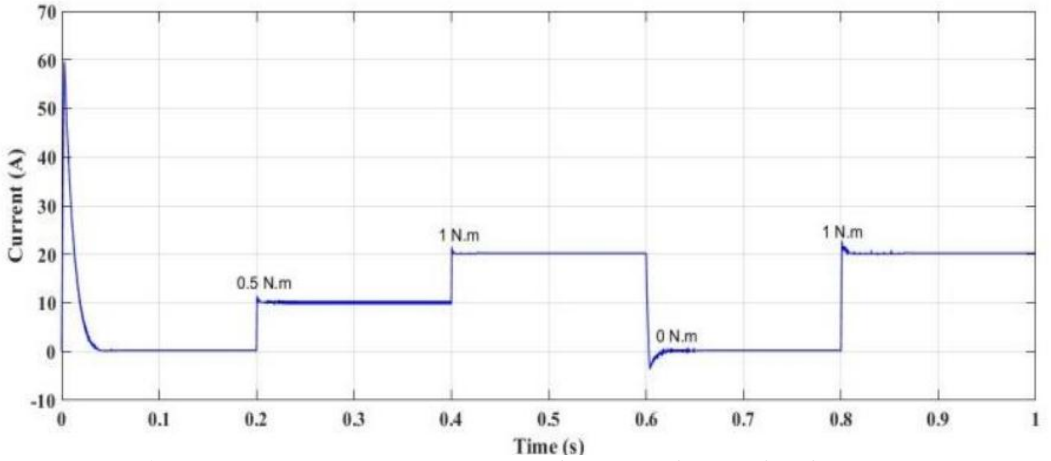

Figure 10 Current responses to the step change load torque

The figure 11 shows that the output waveform of motor reversal control with measured speed performances. In that wave form from 0 sec to 0.5 sec motor is running forward direction with the RPM of 100. After 0.5 sec motor trying to change the direction of speed. In that condition motor running reverse direction with -100 rpm. the motor will not change the direction of rotor in sudden instant, it will take some time to making of braking and reversal. normally 0.15 sec it will take for reversal.

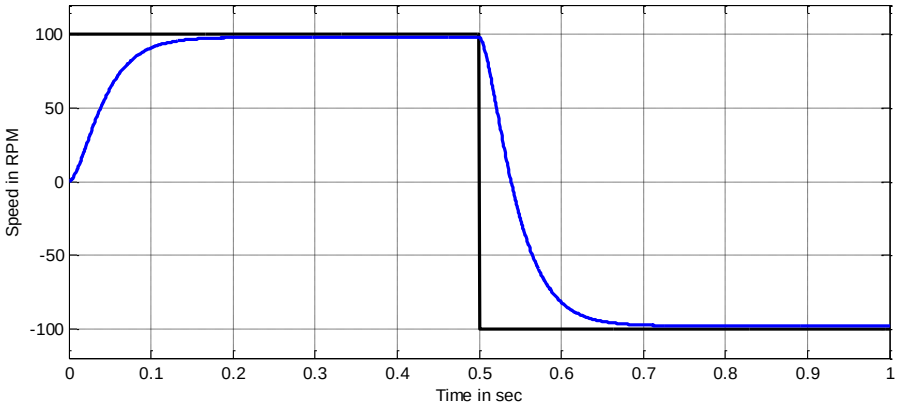

Figure 11 Motor Reversal with Measured speed

The wave form of Motor performance during Reversal and the corresponding speed, current and Torque changes are shown figure 12. From that the waveform 0 sec to 0.5 sec the motor is running forward direction with the speed of 100 rpm. the current of DC motor is nearly 1A and also at starting it will take up to 4 Amps due to the starting current. Now the torque is also 6 N-M. After 0.5 sec the motor trying to change the speed. on that instant the armature current is increasing in negative side -4 amps. The torque also slowly gets to zero and came to -6 N-m.

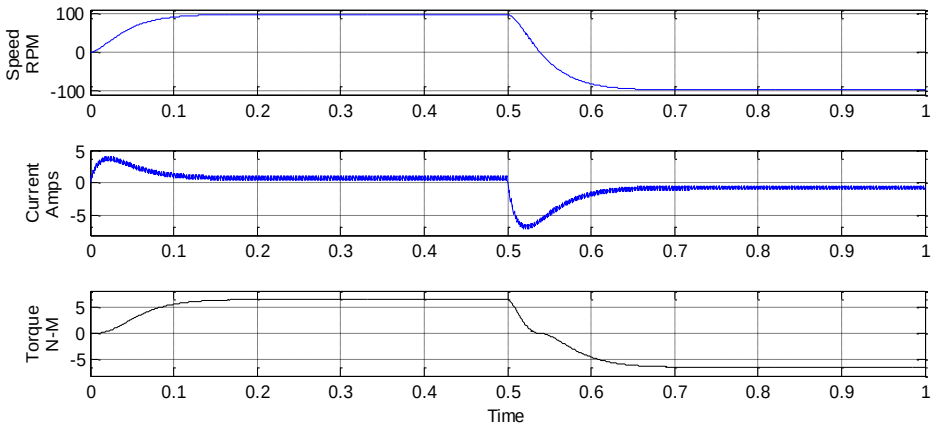

Figure 12 Motor Reversal speed, current and Torque

The wave form 13 shows that the H bridge pulse pattern during forward direction of rotation and reverse direction of rotation. During the forward direction Switch S1 and S4 will be turn on; S2 and S3 will be turned off. After the time period 0.5 sec the switch S1 and S4 gate pulses going to 0, and the switch S2 and S3 will turned on. The wave form 14 shows that the pulse generation duty cycle of 75 percent turn on time and 25 percent turn off time period.

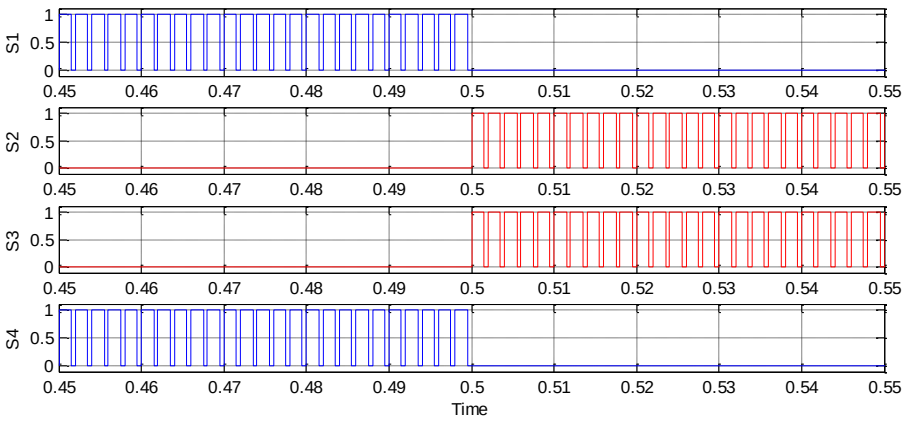

Figure 13 Pulse Patten for H Bridge to motor reversal

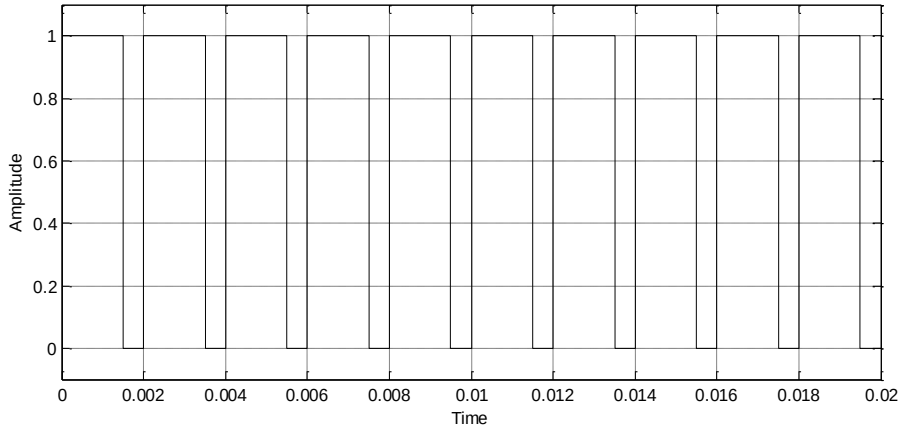

Figure 14 75 percent duty cycle for speed control

Conclusion

In this research work concluded that the DC motor is not suitable for very high precession medical application like laparoscopy device. Because the reference speed and measure speed of the DC motor not aligned properly. Sudden direction change also not applicable in this kind of Brushed DC motor. The reversal of motor taking some delay it will leads to medical damage for patients.

References

1. B. Singh, S. Prakash, A. Pandey and S. K. Sinha, "Intelligent PI Controller for Speed Control of DC Motor,"Int. Journal of Electronic Engineering Research, vol.2, no.1 pp. 87–100, 2010.
2. P. Tripuraa,Y. Srinivasa and K. Babub, "Intelligent Speed Control of DC Motor using ANFIS," Journal of Intelligent & Fuzzy Systems, vol. 26, pp. 223–227, 2014.

3. W. Elsrogy, M. Fkirin and M. Moustafa Hassan, "Speed Control of DC Motor using PID Controller Based on Artificial Intelligence Techniques," IEEE Int. Conf. on Control Decision and Information Technologies (CoDIT) (Tunisia), pp. 196–201, 2013.
4. S. Suman and V. Giri March, "Speed Control of DC Motor using Optimization Techniques Based PID Controller," 2nd IEEE Int. Conf. on Engineering and Technology (ICETECH) (Coimbatore, India), pp. 581–587, 2016.
5. A. Rincon, F. Angulo and F. Hoyos, "Controlling a DC Motor through Lypaunov-like Functions and SAB Technique," International Journal of Electrical and Computer Engineering (IJECE), vol. 8, no. 4, pp. 2180 – 2198, 2018.
6. Premalatha R. and P. Murugesan, "Comparison of Filter with Fuzzy Controlled Three Levels DC-DC Converter Fed Drive," Int. Journal of Engineering Research in Africa, Trans Tech Publications, vol. 14 pp. 63–74, 2015.
7. A. Roy and S. Srivastava, "Design of Optimal PIλDδ Controller for Speed Control of DC Motor Using Constrained Particle Swarm Optimization," IEEE 2016 Int. Conf. on Circuit, Power and Computing Technologies (India), pp. 1–6, 2016.
8. A. Mishra, A. Khanna, N. Singh and V. Mishra, "Speed Control of DC Motor Using Artificial Bee Colony Optimization Technique," Universal Journal of Electrical and Electronic Engineering, vol.1 no.3 pp. 68–75, 2013.
9. T. Amieur, M. Sedraoui and O. Amieur, "Design of Robust Fractional-Order PID Controller for DC Motor Using the Adjustable Performance Weights in theWeighted-Mixed Sensitivity Problem," International Journal of Robotics and Automation (IJRA), vol. 7, no. 2, pp. 108-118, 2018.
10. A. Obed and A. Kadhim, "Multi-Resolution Wavelet PID Speed and Current Controllers of BLDC Motor Based on Invasive Weed Optimization Technique," International Journal of Applied Engineering Research ISSN 0973-4562, vol. 13, no. 8 pp. 6234–6243, 2018.
11. A. Kadhim and A. Obed, "Brushless DC Motor Speed Control Based on PID Controller with 2-DOF and AntiWindup Techniques," 2nd Engineering Conference for Graduate Research Middle Technical University-Electrical Engineering Technical College (Baghdad Iraq), pp 1–14, 2017.
12. A. Saleh and A. Obed, "Speed Control of Brushless DC Motor Based on Fractional Order PID Controller," Int. Journal of Computer Applications, vol. 95, no.4, June 2014.
13. A. Saleh, M. Hussain and S. Klim, "Optimal Trajectory Tracking Control for a Wheeled Mobile Robot Using Fractional Order PID Controller," Journal of University of Babylon Engineering Sciences (Iraq), vol. 26, no.4, pp. 292–306, 2018.
14. S. Sung, J. Lee and I. Lee "Process identification and PID control," (John Wiley & Sons).
15. H. Shin and J. Park, "Anti-Windup PID Controller with Integral State Predictor for Variable-Speed Motor Drives," IEEE Transactions on Industrial Electronics, vol.59, no.3, pp. 1509–1516, 2012.
16. S. Pandey, P. Dwivedi and A. Junghare, "A Newborn Anti-Windup Scheme Based on State Prediction of Fractional Integrator for Variable Speed Motor,"

IEEE 17th Int. Conf. on Control, Automation and Systems (Ramada Plaza Jeju Korea), pp. 663−668, 2017.
17. F. Padula, A. Visioli and M. Pagnoni, "On the Anti-Windup Schemes for Fractional-Order PID Controllers," IEEE Int. Conf.on Power Electronics, Intelligent Control and Energy Systems (Delhi India) pp. 1−4, 2012.
18. S. Pandey, P. Dwivedi and A. Junghare, "Anti-Windup Fractional Order PIλ−PDμ Controller Design for Unstable Process: a Magnetic Levitation Study Case Under Actuator Saturation," Springer Arabian Journal for Science and Engineering vol. 42, no. 12, pp. 5015–5029, 2017.
19. A. Mehrabian and C. Lucas, "A Novel Numerical Optimization Algorithm Inspired from Weed Colonization," Ecological informatics, vol.1, no.4, pp. 355–366, 2006.
20. S. Mekni and B. Fayech, "A Modified Invasive Weed Optimization Algorithm for Multi-Objective Flexible Job Shop Scheduling Problems," Computer Science & Information Technology, pp. 51–60, 2014.
21. M. Khalilpour, N. Razmjooy, H. Hosseini and P. Moallem, "Optimal Control of DC Motor Using Invasive Weed Optimization (IWO) Algorithm," Majlesi Int. Conf. on Electrical Engineering (Iran), January 2011.
22. B. Nayak and S. Sahu, "Parameter Estimation of DC Motor through Whale Optimization Algorithm," International Journal of Power Electronics and Drive System (IJPEDS), vol. 10, no. 1, pp. 83-92, 2019.